Supporting Information

Constructing Fe/Ni Atomic Interfaces in Fe-doped $Ni(OH)_2$ with Single Phase Structure for Efficient Oxygen Evolution

Cheng-Fei Li,[b] Hai-Bo Tang,[b] Jia-Wei Zhao,[c] and Gao-Ren Li[a,*]

[a]*College of Materials Science and Engineering, Sichuan University, Chengdu 610065, China*

[b]*Foshan Xianhu Laboratory of the Advanced Energy Science and Technology Guangdong Laboratory, Xianhu Hydrogen Valley, Foshan 528200, China*

[c]*School of Chemistry, Sun Yat-Sen University, Guangzhou 510275, China*

Email: ligaoren@scu.edu.cn

Experimental Section

Catalyst synthesis. 0.293 g $Ni(NO_3)_2 \cdot 6H_2O$, and 0.5g $C_6H_{12}N_4$ were mixed in 40 mL H_2O under magnetic stirring to form a homogeneous solution. The mixed solution was transferred into a round-bottom flask, and then allowed to react at 80 ºC for different prereaction time (0, 20, 40 and 60 min). After that, 0.1 M $FeCl_2$ (10 mL) were dumped into the above solution, and meanwhile lower stirring speed. Subsequently, the mixture maintained at 80 ℃ for 6 h under refluxing. The product was centrifuged, washed with deionized water for several times and dried at 70 ℃. Finally, the resultant samples were denoted as Fe-doped $Ni(OH)_2$-0, 20, 40 and 60 min according to the prereaction time. Additionally, Fe-doped $Ni(OH)_2$-0 min@CNT and Fe-doped $Ni(OH)_2$-40 min@CNT were synthesized with the same produce, except that 10 mg CNT was added into the precursor resolution before $FeCl_2$ adding.

Physical characterizations. The powder XRD patterns were obtained from a Rigaku SmartLab diffractometer with Cu Kα (λ = 1.5406 Å) radiation operating at 30 kV and 200 mA. The XPS was performed on an ESCA Lab250 X-ray photoelectron spectrometer. The Raman spectra of the materials were obtained with on a RENISHAW inVia instrument using an excitation wavelength of 532 nm. The SEM images were recorded on a Quanta 400FEG instrument. The

transmission electron microscope (TEM) images were collected on JEOL JEM-1400 at 300 kV. Spherical aberration-corrected STEM was carried out on JEM-ARM300F. Inductively coupled plasma atomic emission spectroscopy (ICP-AES) was conducted on a Perkin-Elmer Optima 3300DV ICP spectrometer. XAS characterizations, which included X-ray absorption near-edge structure spectroscopy and extended X-ray absorption fine structure spectroscopy, were performed with Si(111) crystal monochromators at the BL14W1 beamlines at the Shanghai Synchrotron Radiation Facility (SSRF) (Shanghai, China). XAS data were processed with the ATHENA and ARTEMIS software packages.

Electrochemical measurements. All the electrochemical tests were performed in a conventional three-electrode system at CHI 760E electrochemical station, using Hg/HgO electrode as the reference electrode, graphitic carbon rod as the counter electrode and glassy carbon (GC) electrode as the working electrode. Linear sweep voltammetry with scan rate of 5 mV s^{-1} was conducted with IR-compensation in 1.0 M KOH solution. The chronoamperometry measurement was employed to described the long-term stability tests at 10 mA cm^{-2}. The electrochemical impedance spectroscopy measurements were carried out at 0.7 V vs. Hg/HgO in a frequency changing from 100 kHz to 0.01 Hz. Cyclic voltammetry was conducted to probe the double-layer capacitor (C_{dl}) to calculate the electrochemically active surface area (ECSA).

Electrodes preparation: 2.0 mg catalyst were dispersed in 0.9 mL ethanol with 0.1 mL 5 wt% Nafion117 solution under ultrasonication for 30 min. 8 μL of this ink was drop-cast onto a glassy carbon electrode with 0.07 cm^2 area and dried naturally.

Theoretical calculations. The Vienna Ab Initio Package (VASP) was used to conduct all the density functional theory (DFT) calculations within the generalized gradient approximation (GGA) using the Perdew, Burke, and Enzerhof (PBE) formulation[1, 2]. we used the projected augmented wave (PAW) potentials to describe the ionic cores, and take valence electrons into account using a plane wave basis set with a kinetic energy cutoff of 450 eV [3, 4]. Partial occupancies of the Kohn–Sham orbitals were allowed using the Gaussian smearing method and a width of 0.05 eV. The electronic energy was considered self-consistent when the energy change was smaller than 10^{-4} eV. A geometry optimization was considered convergent when the force change was smaller than 0.03 eV/Å. Grimme's DFT-D3 methodology was used to describe the dispersion interactions [5-7]. The equilibrium lattice constants of Si unit cell were optimized when using a 2 × 2 × 1 Monkhorst-Pack k-point grid for Brillouin zone sampling. The free energies were obtained by $G = E_{total} + E_{ZPE}$ - TS, where E_{total}, E_{ZPE} and TS are the ground-state energy, zero-point energies, and entropy terms, respectively, with the latter two taking vibration frequencies from DFT. The U corrections had been employed to calculate the properties.

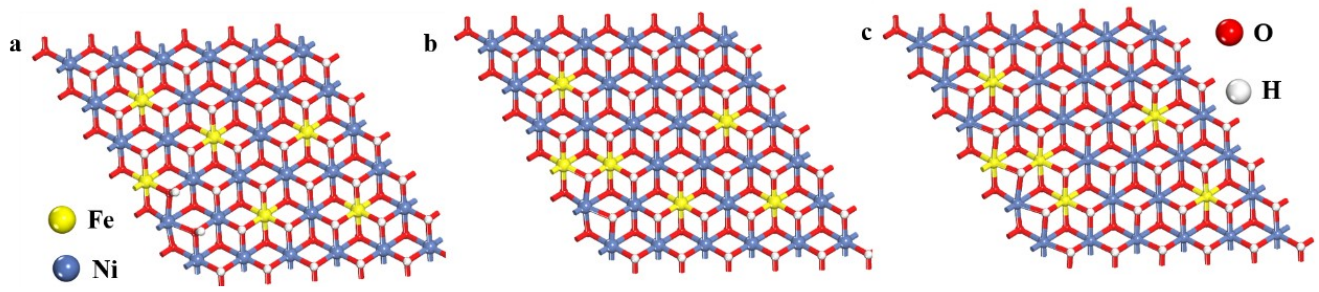

Figure S1. Atomic structure of (a) Fe-doped $Ni(OH)_2$ (Fe1), (b) Fe-doped $Ni(OH)_2$ (Fe2), and (c) Fe-doped $Ni(OH)_2$ (Fe3).

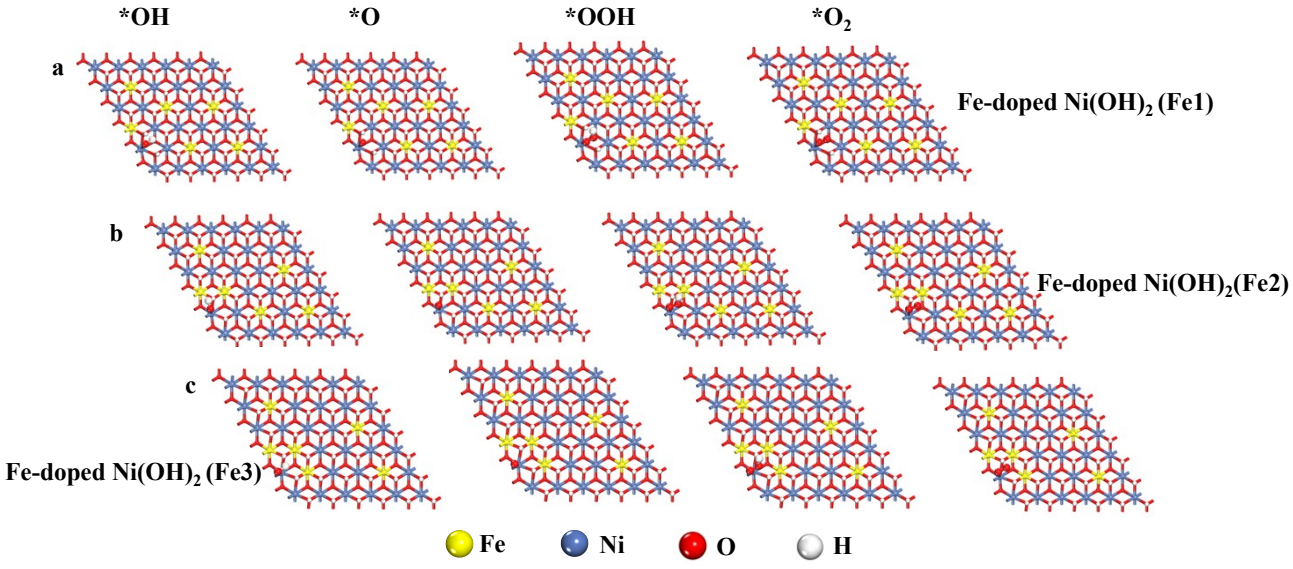

Figure S2. 4e-OER reaction pathway for different intermediates: (a) Fe-doped $Ni(OH)_2$ (Fe1), (b) Fe-doped $Ni(OH)_2$ (Fe2), and (c) Fe-doped $Ni(OH)_2$ (Fe3).

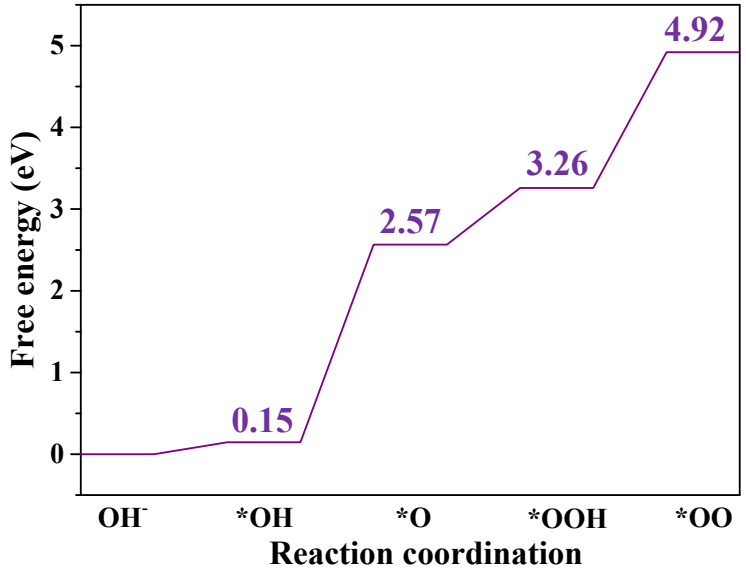

Figure S3. Free energy diagram of Fe-Ni(OH)$_2$ (Fe site) during OER.

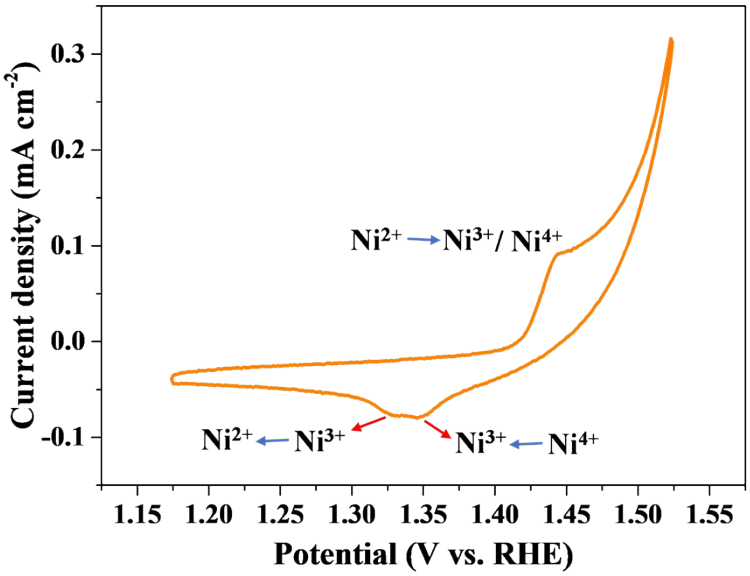

Figure S4. CV curve of Fe-doped Ni(OH)$_2$ during OER.

Figure S5. Optical image of Fe^{2+} color in aqueous solution.

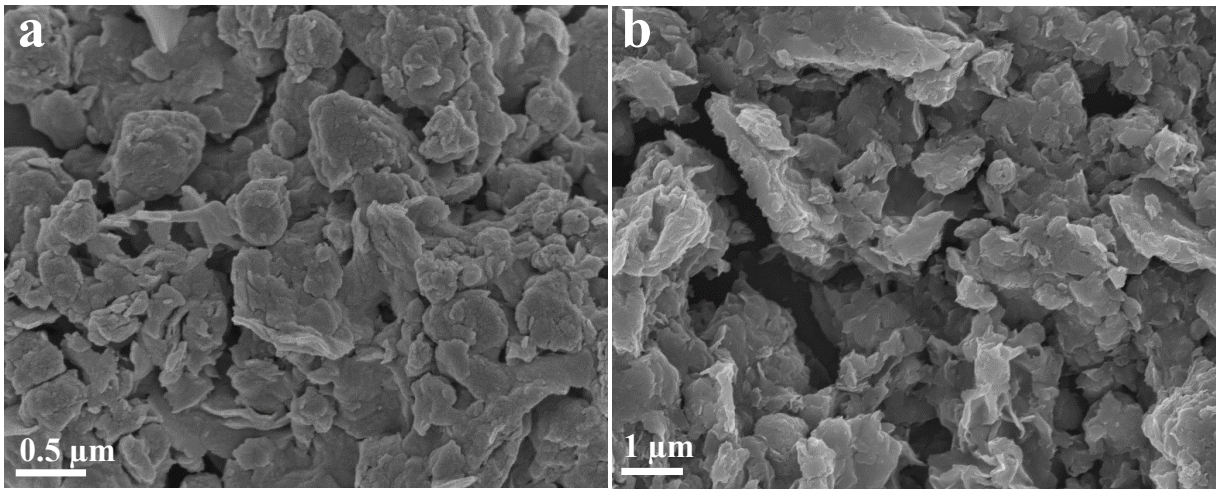

Figure S6. SEM images of (a) Fe-doped $Ni(OH)_2$-0 min and (b) Fe-doped $Ni(OH)_2$-40 min with atomic interface, respectively.

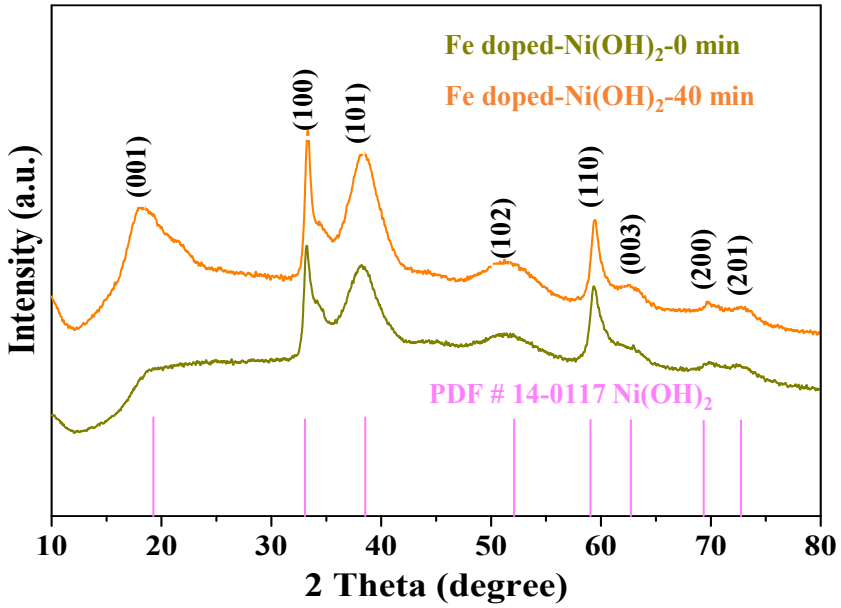

Figure S7. XRD patterns of Fe-doped $Ni(OH)_2$-0 min and Fe-doped $Ni(OH)_2$-40 min with atomic interface.

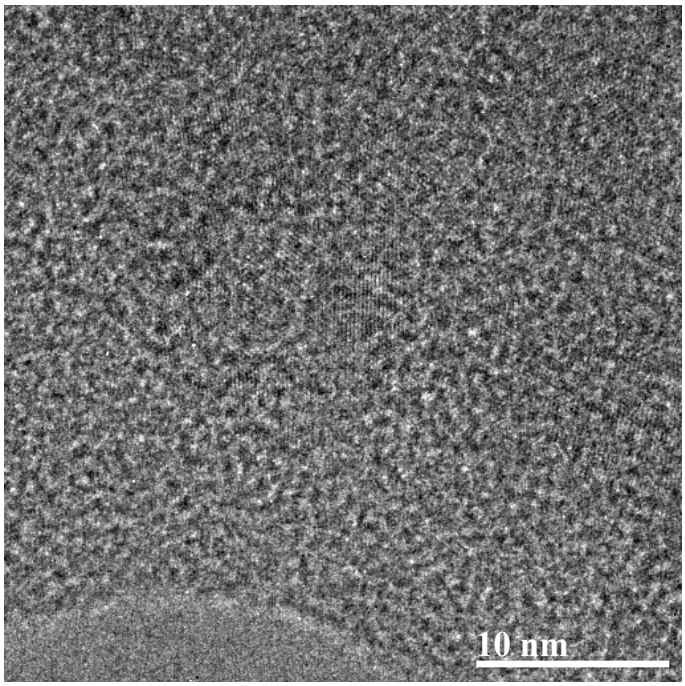

Figure S8. TEM image of Fe-doped $Ni(OH)_2$-0 min.

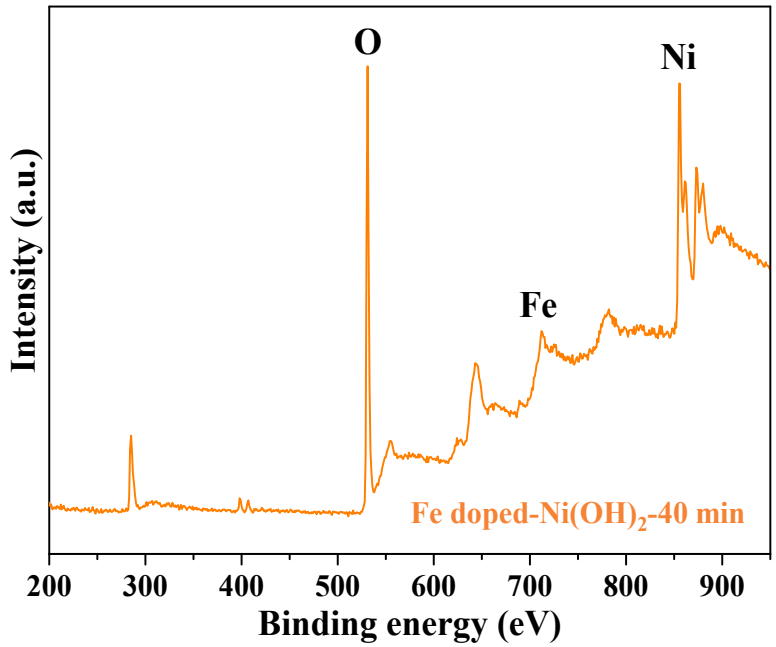

Figure S9. XPS survey spectra of Fe-doped $Ni(OH)_2$-40 min with atomic interface.

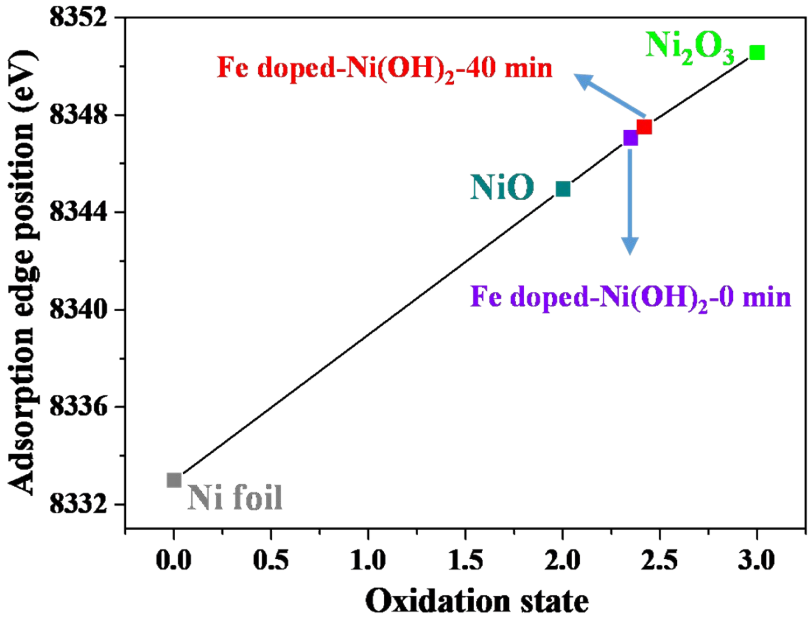

Figure S10. Relationship between Ni K-edge threshold value (E_0) and oxidation state for Fe-doped $Ni(OH)_2$-40 min and reference samples.

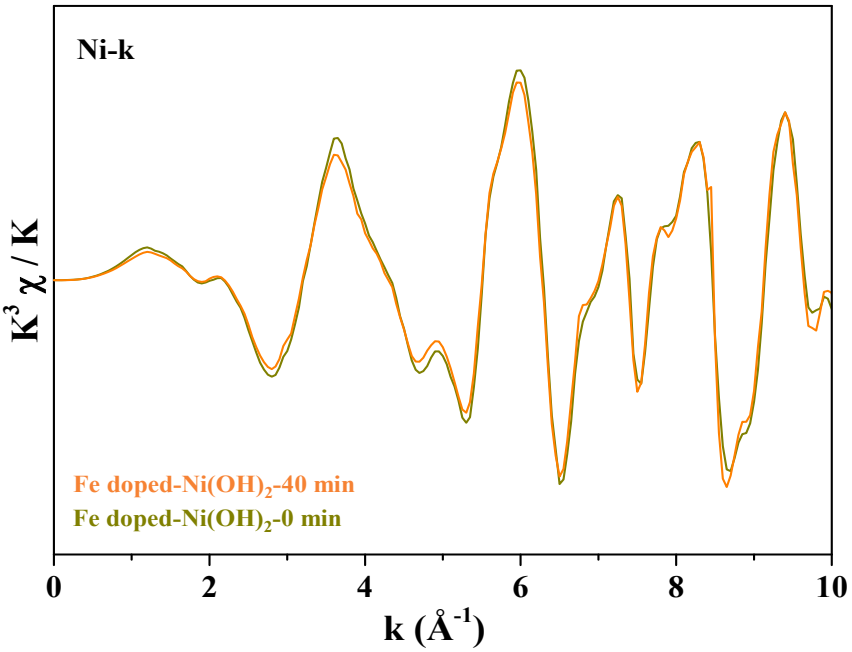

Figure S11. Ni K-edge EXAFS of oscillations of Fe-doped $Ni(OH)_2$-0 min and Fe-doped $Ni(OH)_2$-40 min with atomic interface.

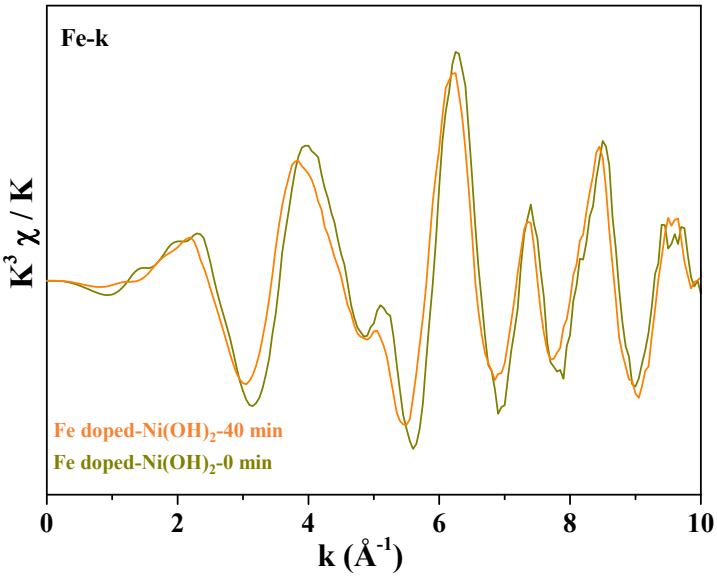

Figure S12. Fe K-edge EXAFS of oscillations of Fe-doped $Ni(OH)_2$-0 min and Fe-doped $Ni(OH)_2$-40 min with atomic interface.

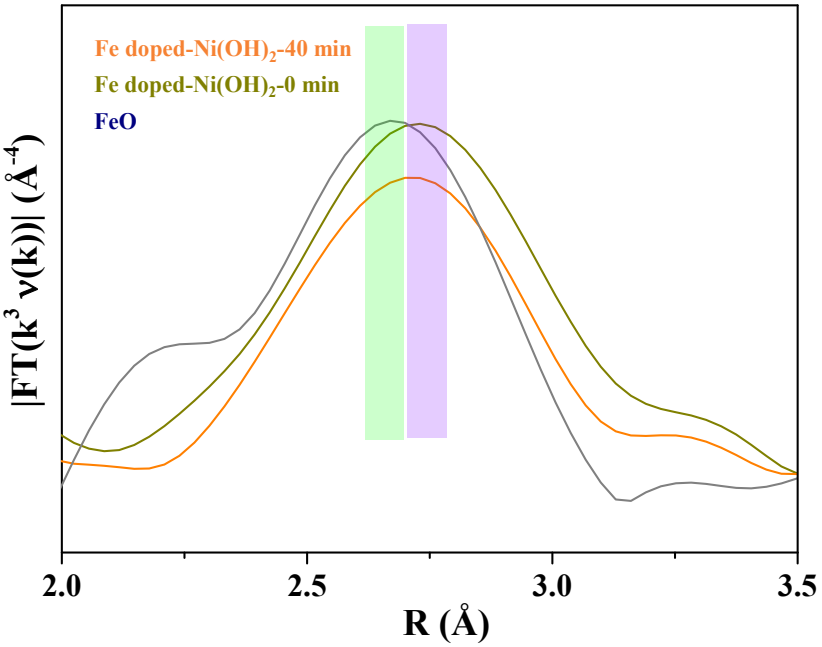

Figure S13. Fourier transform EXAFS spectra of Fe-doped $Ni(OH)_2$-0 min, Fe-doped $Ni(OH)_2$-40 min with atomic interface and FeO.

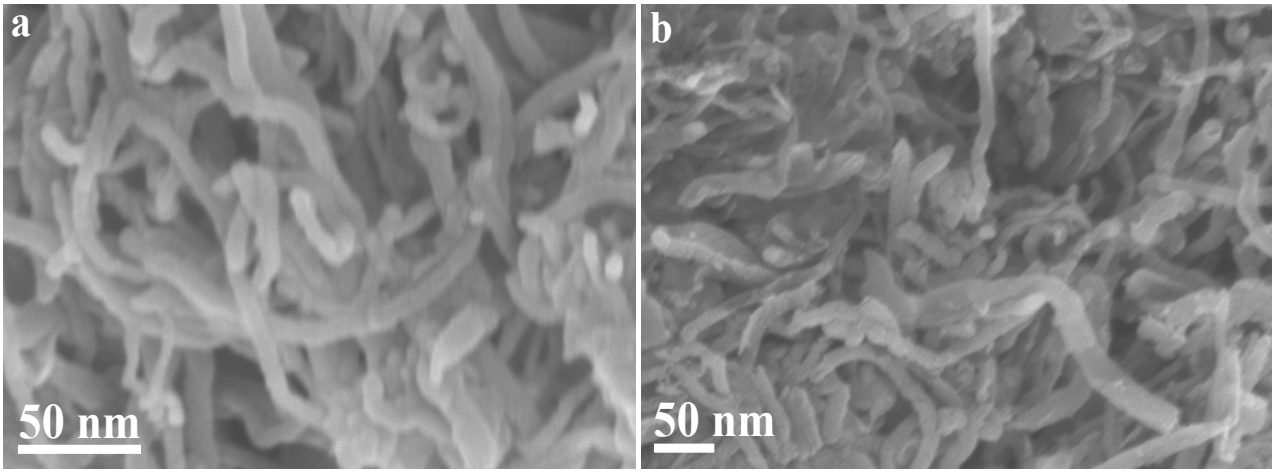

Figure S14. SEM images of (a) Fe-doped $Ni(OH)_2$-0 min and (b) Fe-doped $Ni(OH)_2$-40 min with atomic interface.

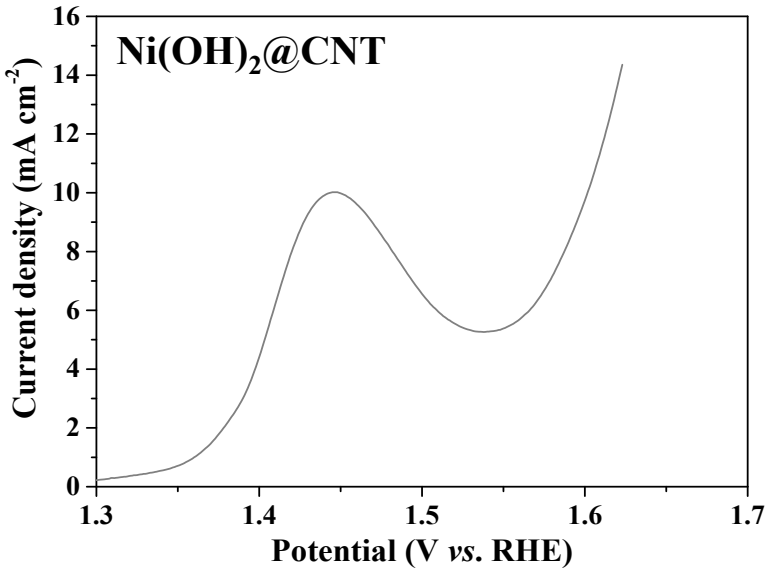

Figure S15. LSV curve of $Ni(OH)_2$@CNT in 1.0 M KOH solution at a scan rate of 5 mV s^{-1} by a typical three-electrode system.

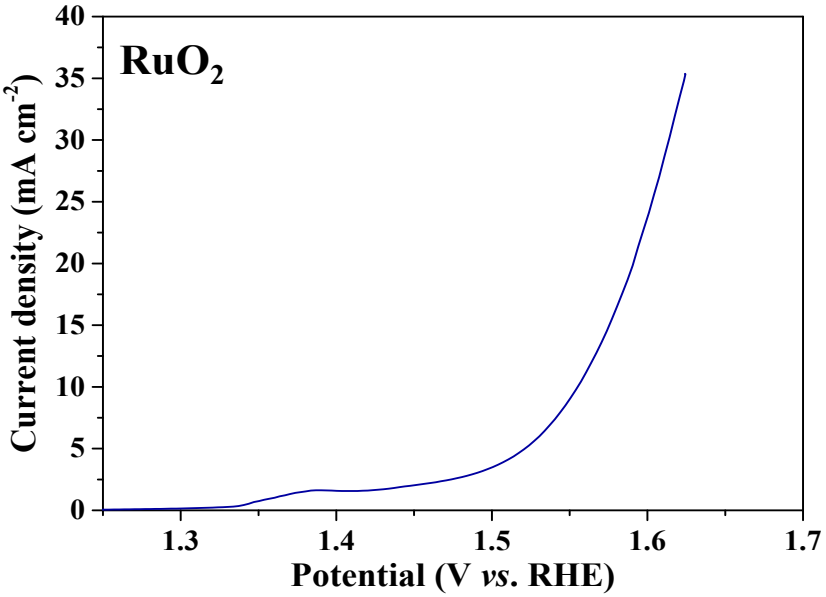

Figure S16. LSV curve of RuO_2 in 1.0 M KOH solution at a scan rate of 5 mV s^{-1} by a typical three-electrode system.

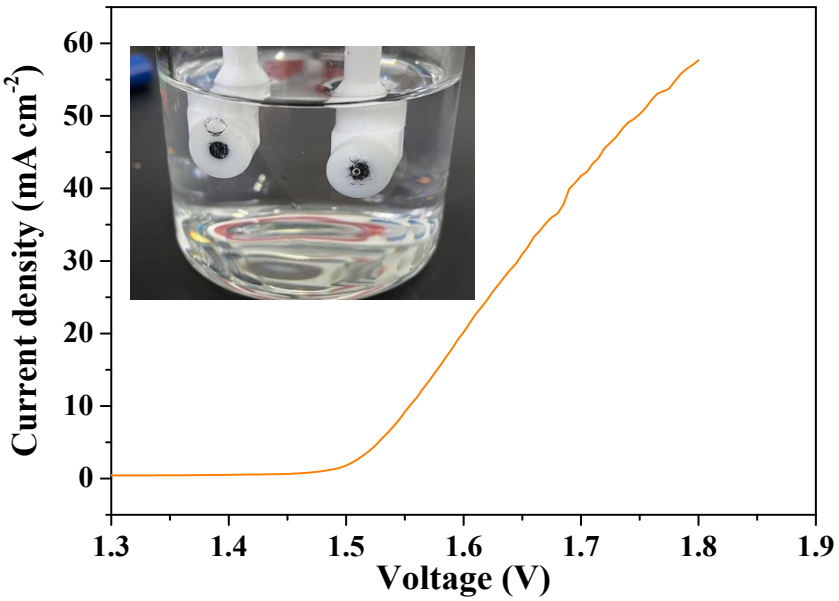

Figure S17. Polarization curve of overall water splitting with Fe-doped $Ni(OH)_2$-40 min as anode and 20% Pt/C as cathode.

Table S1. Comparisons of catalytic performance with reported works.

Catalysts	Overpotential (mV)	Fe/Ni atom ratio	References
Fe-doepd $Ni(OH)_2$-40 min	243	1/10	This work
Fe-enriched $Ni(Fe)O_xH_y$	218	1/2	Nano Lett. 2021, 21, 492−499
sulfated NiFe-LDH	219	19.8/70.7	Chem. Eng. J. 2021, 426 130873
hcp-NiFe@NCs	226	5/27	Angew. Chem. Int. Ed. 2019, 58, 6099 –6103
MIL-53(FeNi)/NF	233	1/1	Adv. Energy Mater. 2018, 8, 1800584
NiFe LDH-0.20 M	243	~1/2	ACS Catal. 2020, 10, 11127−11135
PM-LDH	230	~1/3	Adv. Energy Mater., 2019, 9, 1900881.
Ni–Fe LDH DSNC	246	100/93	Adv. Mater. 2020, 32, 1906432
NiFe-LDH	247	1/2	ACS Catal. 2020, 10, 1886−1893
NiFe LDH-Ni(III)Li	248	1/4	J. Mater. Chem. A, 2020, 8, 26130
Ni–Fe–Se	249	80/119	Adv. Mater. 2021, 33, 2103004
CF-PBA-400	254	1/1	ACS Catal. 2022, 12, 3138−3148
NiFe SA	270	3/7	Nat. Commun. 2021, 12, 1-3
$Fe_{1.0}Co_{1.1}Ni_{1.4}$–NC	290	5/7	J. Mater. Chem. A 2020, 8, 9021
S-(Ni,Fe)OOH	300	--	Energy Environ. Sci. 2020, 13, 3439
Fe–NiNC-50	430	~1/2	Nano Energy 2020, 71, 104597
$Ni_{66}Fe_{34}$-NC	467	17/33	Appl. Catal. B: Environ. 274, 2020, 119091

Table S2. Comparisons of catalytic performance for overall water splitting with reported works.

catalysts	Voltage (V)	References
Fe-doepd $Ni(OH)_2$-40 min@CNT	1.55	This work
NiVIr LDH	1.49	ACS Energy Lett. 2019, 4, 1823−1829
MoS_2−Ni_3S_2	1.50	ACS Catal. 2017, 7, 2357−2366
NiCoP/CC	1.52	ACS Catal. 2017, 7, 4131−4137
Cu_3P/Ni_2P@CF	1.56	Chem. Eng. J. 2022, 448, 137706
Fe-doped NiSe NSs/CNTs	1.57	J. Mater. Chem. A 2022, 10, 3102
NiCoP	1.58	Nano Lett. 2016, 16, 7718−7725
$Co_{0.9}S_{0.58}P_{0.42}$	1.59	ACS Nano 2017, 11, 11031-11040
Co_4S_3/Mo_2C-N SC	1.62	Appl. Catal. B: Environ. 2020, 260, 118197
CoFeZr oxides	1.63	Adv. Mater. 2019, 31, 1901439
MoS_2-NiS_2/NGF	1.64	Appl. Catal.B: Environ. 2019, 254, 15–25

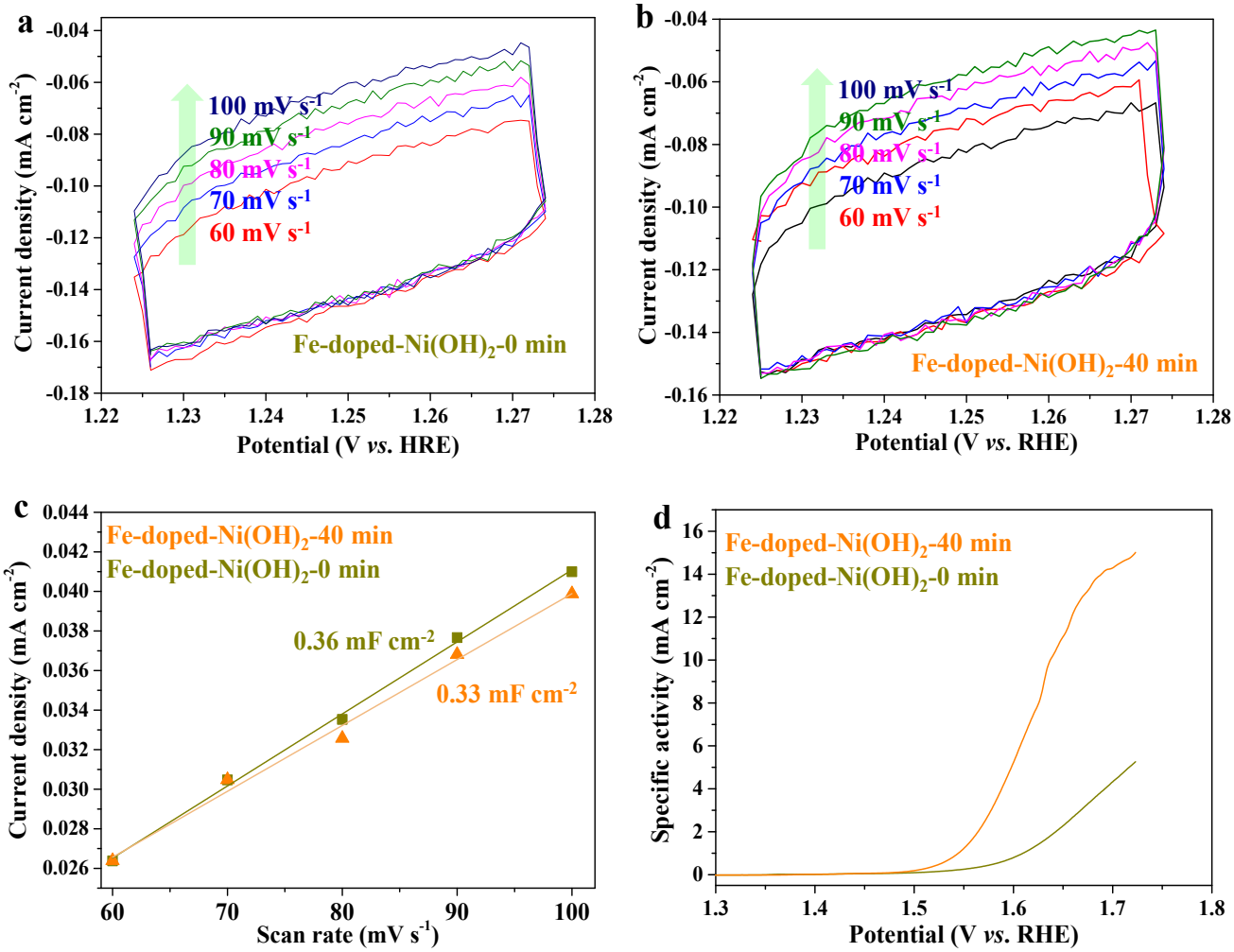

Figure S18. Cyclic voltammetry curves of (a) Fe-doped $Ni(OH)_2$-0 min and (b) Fe-doped $Ni(OH)_2$-40 min, respectively; (c) The plot of capacitive current density as a function of scan rate; (d) LSV curves of Fe-doped $Ni(OH)_2$-0 min and Fe-doped $Ni(OH)_2$-40 min in 1.0 M KOH solution at a scan rate of 5 mV s^{-1} by a typical three-electrode system.

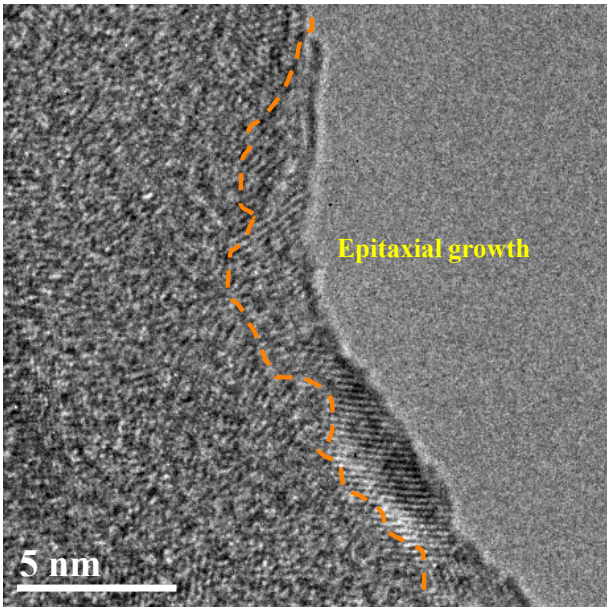

Figure S19. TEM image of Fe-doped $Ni(OH)_2$-40 min after cycling test.

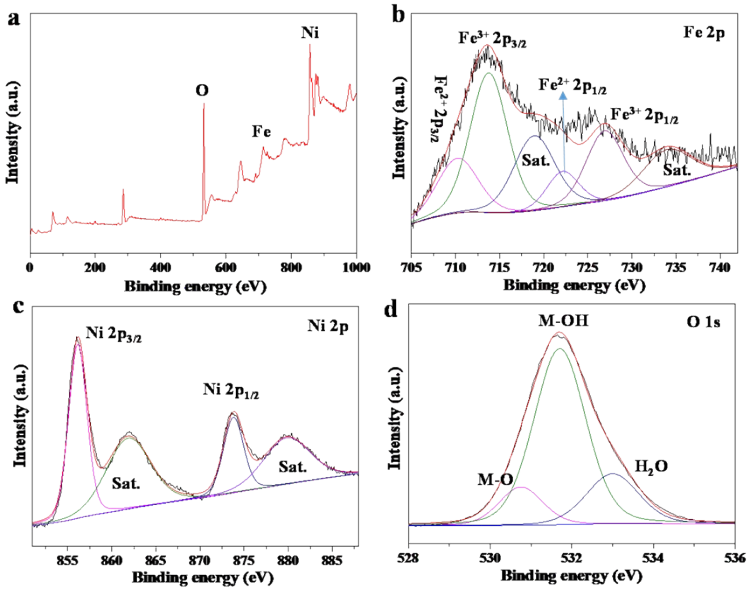

Figure S20. (a) XPS survey spectra, (b-d) XPS spectra of Fe 2p, Ni 2p and O 1s of Fe-doped $Ni(OH)_2$-40 min after cycling test.

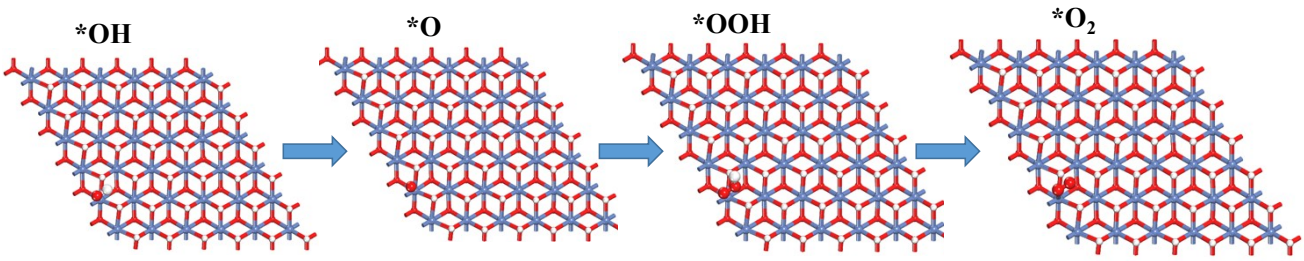

Figure S21. 4e-OER reaction pathway for different intermediates on $Ni(OH)_2$.

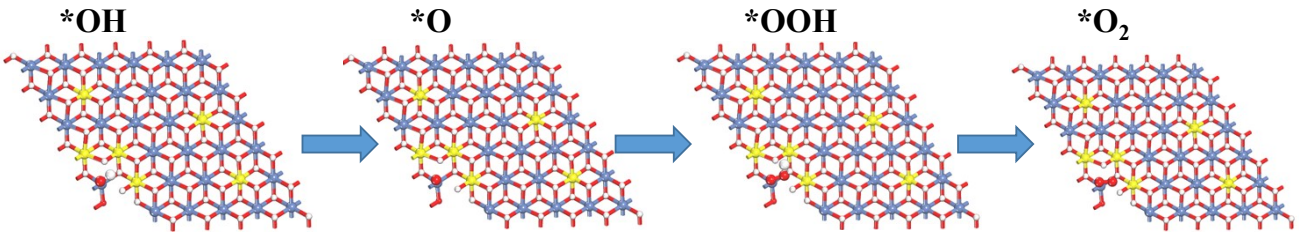

Figure S22. 4e-OER reaction pathway for different intermediates on Fe-doped $Ni(OH)_2$-Fe3-V_{Ni}.

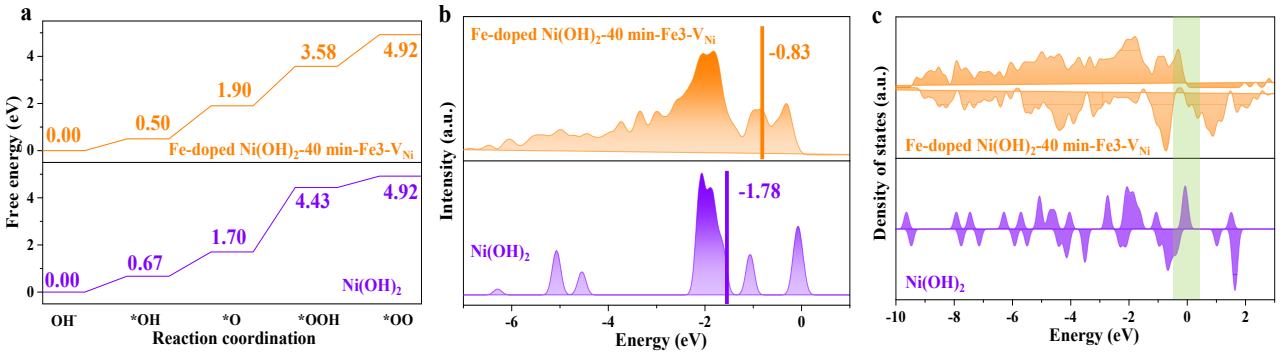

Figure S23. a) Free energy diagram; b) Band center positions for Ni 3d orbitals were also marked; c) Density of states of different samples.

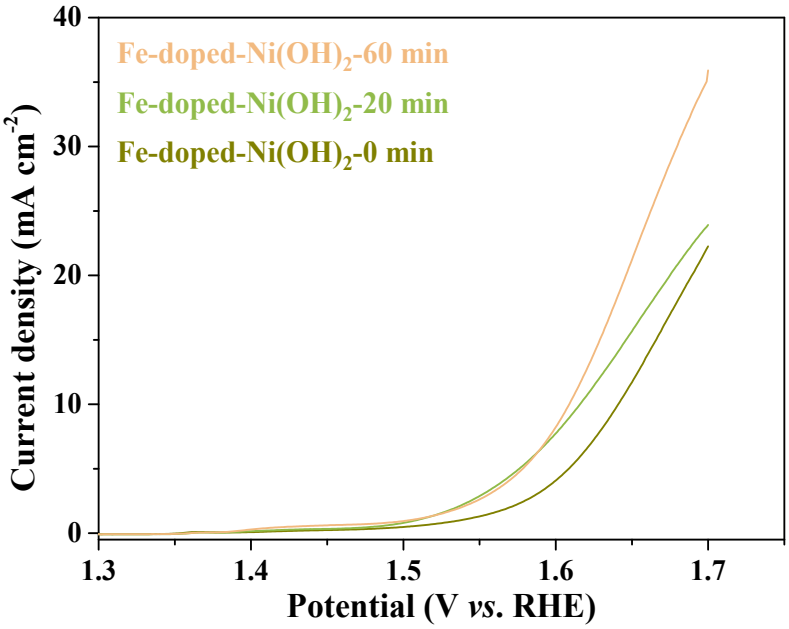

Figure S24. Polarization curves of various pre-reaction time samples in 1.0 M KOH solution at a scan rate of 5 mV s^{-1} by a typical three-electrode system.

References

1. N. Acerbi, S. E. Tsang, G. Jones, S. Golunski, P. Collier, *Angew. Chem. Int. Ed.* **2013**, *125*, 7891-7895.
2. G. Kresse, J. Furthmüller, *Phys. Rev. B* **1996**, *54*, 11169.
3. J. P. Perdew, K. Burke, M. Ernzerhof, *Phys. Rev. Lett* **1996**, *77*, 3865.
4. G. Kresse, D. Joubert, *Phys. Rev. B* **1999**, *59,* 1758.
5. Blöchl, P. E. Projector augmented-wave method, *Phys. Rev. B* **1994**, *50*, 17953.
6. S. Grimme, J. Antony, S. Ehrlich, H. Krieg, *J. Chem. Phys.* **2010**, *132*, 154104.
7. G. Henkelman, B. P. Uberuaga, H. Jónsson, *J. Chem. Phys.* **2000**, *113*, 9901-9904.